Etched beam splitters in InP/InGaAsP

Erik J. Norberg,[1,*] John S. Parker,[1] Steven C. Nicholes,[2] Byungchae Kim,[1] Uppiliappan Krishnamachari,[1] and Larry A. Coldren[1]

[1]*Department of Electrical and Computer Engineering,University of California, Santa Barbara, CA, USA*
[2]*Department of Materials,University of California, Santa Barbara, CA, USA*
**norberg@ece.ucsb.edu*

Abstract: An etched beam splitter (EBS) photonic coupler based on frustrated total internal reflection (FTIR) is designed, fabricated and characterized in the InP/InGaAsP material system. The EBS offers an ultra compact footprint (8x11 μm) and a complete range of bar/cross coupling ratio designs. A novel pre-etching process is developed to achieve sufficient depth of the etched coupling gaps. Fabricated EBS couplers demonstrate insertion loss between 1 and 2.6 dB with transmission (cross-coupling) ≤ 10%. The results show excellent agreement with 3D finite-difference time-domain (FDTD) modeling. The coupling of EBS has weak wavelength dependence in the C-band, making it suitable for wavelength division multiplexing (WDM) or other wide bandwidth applications. Finally, the EBS is integrated with active semiconductor optical amplifier (SOA) and phase-modulator components; using a flattened ring resonator structure, a channelizing filter tunable in both amplitude and center frequency is demonstrated, as well as an EBS coupled ring laser.

©2011 Optical Society of America

OCIS codes: (130.0130) Integrated optics; (230.1360) Beam splitters; (250.5300) Photonic integrated circuits; (230.5750) Resonators

References and links

1. C.-H. Chen, J. Klamkin, S. C. Nicholes, L. A. Johansson, J. E. Bowers, and L. A. Coldren, "Compact beam splitters with deep gratings for miniature photonic integrated circuits: design and implementation aspects," Appl. Opt. **48**(25), F68–F75 (2009).
2. R. Grover, V. Van, T. A. Ibrahim, P. P. Absil, L. C. Calhoun, F. G. Johnson, J. V. Hryniewicz, and P.-T. Ho, "Parallel-Cascaded Semiconductor Microring Resonators for High-Order and Wide-FSR Filters," J. Lightwave Technol. **20**(5), 872–877 (2002).
3. A. Yalcin, K. C. Popat, J. C. Aldridge, T. A. Desai, J. Hryniewicz, N. Chbouki, B. E. Little, Oliver King, V. Van, Sai Chu, D. Gill, M. Anthes-Washburn, M. S. Unlu, and B. B. Goldberg, "Optical sensing of biomolecules using microring resonators," IEEE J. Sel. Top. Quantum Electron. **12**(1), 148–155 (2006).
4. Y. Ma, S. Park, L. Wang, and S. T. Ho, "Ultracompact multimode interference 3-dB coupler with strong lateral confinement by deep dry etching," IEEE Photon. Technol. Lett. **12**(5), 492–494 (2000).
5. Y. Shi, S. He, and S. Anand, "Ultracompact directional couplers realized in InP by utilizing feature size dependent etching," Opt. Lett. **33**(17), 1927–1929 (2008).
6. S. J. Choi, K. Djordjev, S. J. Choi, P. D. Dapkus, W. Lin, G. Griffel, R. Menna, and J. Connolly, "Microring resonator vertically coupled to buried heterostructure bus waveguides," IEEE Photon. Technol. Lett. **16**(3), 828–830 (2004).
7. J. S. Osinski, C. E. Zah, R. Bhat, R. J. Contolini, E. D. Beebe, T. P. Lee, K. D. Cummings, and L. R. Harriott, "Miniature integrated optical Beam-Splitter in AlGaAs/GaAs ridge waveguides," Electron. Lett. **23**(21), 1156–1158 (1987).
8. L. Li, G. P. Nordin, J. M. English, and J. Jiang, "Small-area bends and beamsplitters for lowindex-contrast waveguides," Opt. Express **11**(3), 282–290 (2003).
9. B. Kim, and N. Dagli, "Compact Micro Resonators with Etched Beam Splitters and Total Internal Reflection Mirrors," in *Integrated Photonics Research and Applications/Nanophotonics*, Technical Digest (CD) (Optical Society of America, 2006), paper IWB.
10. N. R. Huntoon, M. P. Christensen, D. L. MacFarlane, G. A. Evans, and C. S. Yeh, "Integrated photonic coupler based on frustrated total internal reflection," Appl. Opt. **47**(30), 5682–5690 (2008).
11. S. Zhu, A. W. Yu, D. Hawley, and R. Roy, "Frustrated total internal reflection: a demonstration and review," Am. J. Phys. **54**(7), 601–607 (1986).

#137249 - $15.00 USD Received 26 Oct 2010; revised 17 Dec 2010; accepted 22 Dec 2010; published 5 Jan 2011

12. Y. Qian, J. Song, S. Kim, and G. P. Nordin, "Compact 90 ° trench-based splitter for silicon-on-insulator rib waveguides," Opt. Express **15**(25), 16712–16718 (2007).
13. B. Kim, and N. Dagli, "Submicron Etched Beam Splitters Based on Total Internal Reflection in GaAs–AlGaAs Waveguides," J. Lightwave Technol. **28**(13), 1938–1943 (2010).
14. E. Norberg, J. Parker, U. Krishnamachari, R. Guzzon, and L. Coldren, InGaAsP/InP based Flattened Ring Resonators iwth Etched Beam Splitters," in *Conference on Integrated Photonics and Nanophotonics Research and Applications Nanophotonics*, Technical Digest (CD) (Optical Society of America, 2009), paper IWB.
15. U. Krishnamachari, S. Ristic, C.-H. Chen, L. Johansson, A. Ramaswamy, J. Klamkin, E. Norberg, J. Bowers, and L. Coldren, "InP/InGaAsP-Based Integrated 3-dB Trench Couplers for Ultra-Compact Coherent Receivers," IEEE Photon. Technol. Lett. (to be published).
16. R. H. Renard, "Total reflection: a new evaluation of the Goos–Hänchen shift," J. Opt. Soc. Am. **54**(10), 1190–1197 (1964).
17. J. Parker, E. Norberg, R. Guzzon, S. Nicholes, and L. Coldren, "High verticality InP/InGaAsP etching in $Cl_2/H_2/Ar$ ICP for photonic integrated circuits," J. Vac. Sci. Technol. B (to be published).
18. S. Bouchoule, G. Patriarche, S. Guilet, L. Gatilova, L. Largeau, and P. Chabert, "Sidewall Passivation Assisted by a Silicon Coverplate during Cl_2-H_2 HBr Inductively Coupled Plasma Etching of InP for Photonic Devices," J. Vac. Sci. Technol. B **26**(2), 666–675 (2008).
19. S. Rommel, J.-H. Jang, W. Lu, G. Cueva, L. Zhou, I. Adesida, G. Pajer, R. Whaley, A. Lepore, Z. Schellanbarger, and J. H. Abeles, "Effect of H_2 on the etch profile of InP/InGaAsP alloys in $Cl_2/Ar/H_2$ inductively coupled plasma reactive ion etching chemistriesfor photonic device fabrication," J. Vac. Sci. Technol. B **20**(4), 1327–1330 (2002).
20. E. Norberg, R. Guzzon, and L. Coldren, "Programmable Photonic Filters Fabricated with Deeply Etched Waveguides," in *Proceedings of IEEE Conference on Indium Phosphide and Related Materials*, (IEEE Photonics Society, Newport beach, CA, 2009), pp. 163–166.
21. E. J. Skogen, J. W. Raring, G. B. Morrison, C. S. Wang, V. Lal, M. L. Masanovic, and L. A. Coldren, "Monolithically integrated active components: a quantum-well intermixing approach," IEEE J. Sel. Top. Quantum Electron. **11**(2), 343–355 (2005).
22. E. Norberg, R. S. Guzzon, S. C. Nicholes, J. S. Parker, and L. A. Coldren, "Programmable Photonic Lattice Filters in InGaAsP–InP," IEEE Photon. Technol. Lett. **22**(2), 109–111 (2010).
23. C. K. Madsen, and J. H. Zhao, *Optical Filter Design and Analysis: A Signal Processing Approach*, (Wiley-Interscience 1999), Chap. 6.

1. Introduction

The optical coupler is a key component for photonic integration. Desirably the coupler should have: low loss, variable bar/cross splitting ratio designs, a compact footprint and be easily integrated with other photonic components on-chip. Traditional coupler designs are the y-branch, multi-mode interference (MMI), and directional coupler. For many applications a small foot-print directly translates into higher performance; this includes: short optical delays for linear RF-receivers [1], large free-spectral range (FSR) of micro resonators used as add/drop filters in wavelength division multiplexing (WDM) applications [2], and high sensitivity for micro-rings used in biosensing [3]. The y-branch and MMI coupler is typically limited in compactness, where the smallest MMI coupler to date is 20 μm long, but also very sensitive to fabrication variations [4]. Thus, for compact integration, the directional couplers are most commonly utilized [2,5]. However, when the length of the direction coupler is decreased the coupling gap must be made extremely small in order to obtain any significant coupling. For lateral directional couplers this implies the use of electron beam lithography (EBL) and very small processing tolerances. While the coupling gap can be controlled precisely in vertical directional couplers, this design has the disadvantage of multiple waveguide stacks, thus demanding complicated fabrication often with additional material re-growths [6]. Ultimately, for compact coupler designs, the cross coupling of direction couplers is still limited to a few percent. On the contrary, the etched beam splitter (EBS) has been proposed and investigated as an ultra compact coupler that offers a complete range of power splitting ratios independent of size [7–10]. The EBS is the monolithic version of a conventional bulk prism beam splitter, with the coupling mechanism based on the same physical phenomena of evanescent coupling through frustrated total internal reflection (FTIR) [11]. The first EBS was realized over two decades ago [7], but with very limited success due to immature fabrication technology. More recently, the EBS has demonstrated better performance with silicon-on-insulator (SOI) [12], AlGaAs [13] and polymer based waveguide

#137249 - $15.00 USD Received 26 Oct 2010; revised 17 Dec 2010; accepted 22 Dec 2010; published 5 Jan 2011
(C) 2011 OSA

platforms [8]. We have extended to the InP/InGaAsP material system in order to integrate the EBS coupler with an active gain platform [14,15]. Here, we report on the modeling, fabrication and characterization of such EBS couplers in InP/InGaAsP. Furthermore, taking advantage of the active gain and phase modulation provided by the InP/InGaAsP material system, we have integrated the EBS in a novel flattened ring resonator structure to create a channelizing filter tunable in both center wavelength and extinction ratio.

2. EBS design and modeling

The general design of the EBS is two intersecting waveguides with a narrow lower index gap at the crossing point, making it a symmetric 2x2 coupler, as shown in Fig. 1(a). For total internal reflection (TIR) to take place, the incident angle of the waveguides (Θ_i) needs to be greater than the critical angle (Θ_c). The power coupling across the EBS gap is facilitated by the evanescent wave present during TIR. In this work we used a 300 nm thick InGaAsP 1.3Q waveguide layer surrounded by InP cladding. For the lateral optical confinement we utilize air cladding by etching through the waveguide layer, as shown Fig. 1(c). For this waveguide design and using an air filled EBS gap, Θ_c is approx. 18°. The deeply etched waveguides provide strong lateral optical confinement and robust fabrication in any crystallographic direction due to the sole use of dry etching. For smaller resonator sizes with reduced ring radii, the strong optical confinement is crucial to avoid excess radiation loss from waveguide bends.

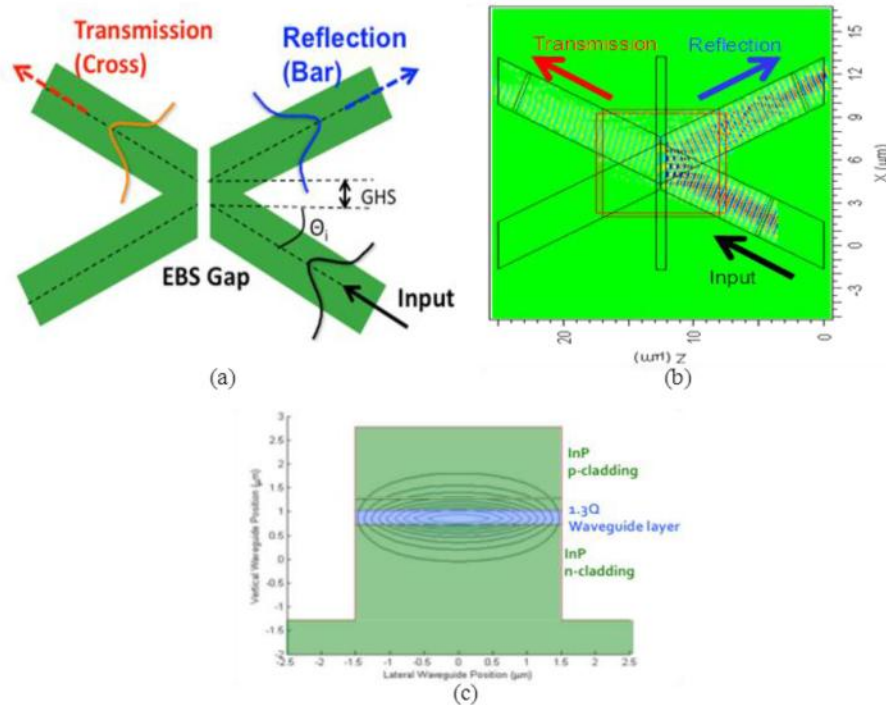

Fig. 1. (a) Schematic of the EBS coupler illustrating the basic design parameters, incident angle (Θ_i) of the input and output waveguides, EBS air gap for evanescent coupling and the Goos-Hanchen shift (GHS) between input and output waveguides. (b) FDTD simulation showing the magnetic field intensity $\left|H_y\right|$. (c) Deeply etched InP/InGaAsP waveguide, with the calculated fundamental mode superimposed.

Qualitatively the evanescent coupling behavior of the EBS can be described with a simple analytical plane-wave model derived from the Fresnel equations [10]. Quantitatively however,

#137249 - $15.00 USD Received 26 Oct 2010; revised 17 Dec 2010; accepted 22 Dec 2010; published 5 Jan 2011
(C) 2011 OSA

this method is only valid in the limiting cases of very weakly guided modes, i.e. when the modal plane wave spectrum is narrow and can be approximated with a single plane wave. For integrated optics this is seldom the case, thus, a more rigorous approach is needed. So far, most predictions on EBS performance has been done using numerical 2D-FDTD simulations [8–10,14]. Some full 3D-FDTD treatment of EBS structure has recently been reported [12,13]. The trade-off in the 2D versus 3D treatment is the computational intensity in the full 3D case versus the fact that the 2D simulations do not account for any transverse effects, such as transverse modal diffraction or slanted EBS mirrors. Here, we make use of and compare the 2D- and 3D-FDTD simulations when designing InP/InGaAsP based EBS couplers. For the 2D-FDTD simulations, the effective index of the waveguide is calculated to be 3.24 using the effective index method, with the surrounding lateral cladding and the EBS air gap being 1. For the 2D simulations, a 10 nm mesh size was used with a time step of 2.3×10^{-17} s, while in the 3D simulations a slightly larger 20 nm mesh size with a 3.3×10^{-17} s time step was used, to reduce computation time. The 20 nm is still much smaller than the minimum feature size of the 300 nm EBS air gap. Hence, numerical errors from the mesh generation should be insignificant. Figure 1(c) shows the FDTD simulation with the evanescent coupling across the air gap.

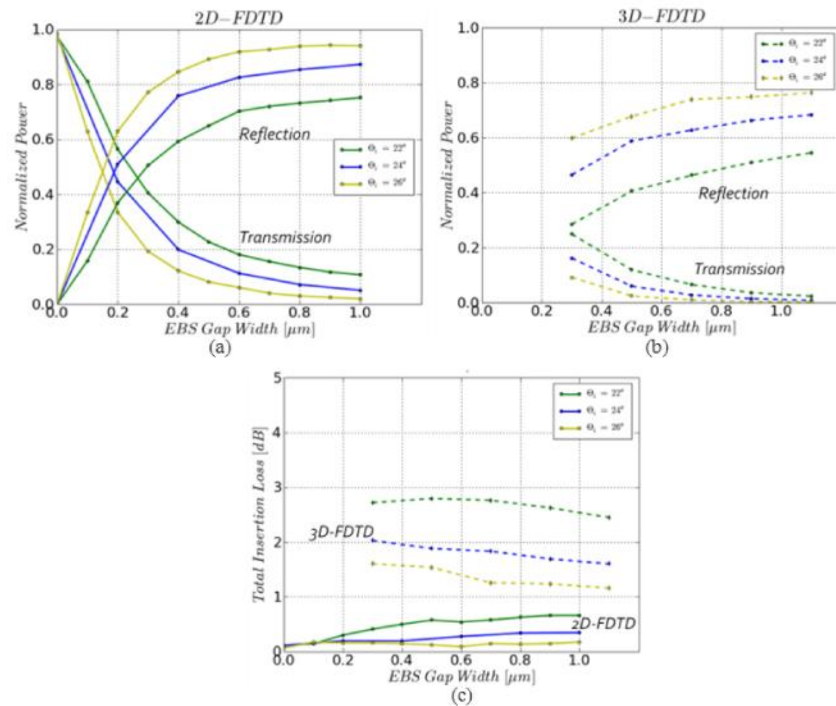

Fig. 2. Power coupling ratios as a function of EBS gap width for different incident angles (Θ_i), (a) 2D- and (b) 3D-FDTD simulations. (c) Total insertion loss of the EBS coupler as a function of gap width for different incident angles, 2D- (solid) and 3D-FDTD simulations (dashed).

The EBS power splitting for different incident angles and air gap widths are shown in Fig. 2(a,b). The trends for the 2D and 3D simulations are consistent; the reflection (bar) component is reduced in favor of a larger transmission (cross) component when the incident angle or gap width is decreased. This is also intuitively expected from the FTIR evanescent field behavior; i.e., the rate of exponential power decay in the EBS gap decreases as the incident angle approaches the critical angle, and a narrower gap corresponding to a shorter decay distance. The obvious discrepancy between the 2D and 3D simulations is seen in the absolute powers, in other words, the insertion loss, shown in Fig. 2(c). The 3D case indicates

#137249 - $15.00 USD Received 26 Oct 2010; revised 17 Dec 2010; accepted 22 Dec 2010; published 5 Jan 2011
(C) 2011 OSA

a much more severe insertion loss compared to the 2D case. This discrepancy can be attributed to transverse modal effects, not accounted for in the 2D simulations. This includes the fact that for the relatively narrow transverse mode profile (i.e. wide transverse plane wave spectrum), as shown in Fig. 1(c), a part of the transverse mode does not obey TIR at the EBS gap. Also, for the transmitted (cross) component, transverse diffraction in the EBS gap results in additional loss. Thus, the insertion loss found in the 3D simulations is rather inherent to our InGaAsP waveguide design. Comparably, using a less confined waveguide mode, lower EBS insertion loss can be achieved [8,12]. The drawback of a wider transverse modal waveguide design lies in that it requires a deeper etched EBS gap, which in this work is the limiting factor of the fabrication process, as will be shown in the following section (EBS fabrication). While the 3D simulations will provide more reliable predictions about the absolute power coupling, the 2D-FDTD is still a good compliment when investigating effects in the lateral plane due to the much shorter simulation time. 2D simulations were thus utilized in optimizing the Goos-Hänchen shift (GHS) [16]. The GHS was accounted for by slightly displacing the reflected waveguide relative to the incident waveguide, as shown in Fig. 1(a). When designing the EBS coupling ratio we note that larger incident angles predict lower insertion loss, as shown in Fig. 2(c). This can be qualitatively explained by the modal profile, where a greater part of the lateral mode profile (or equivalent plane wave spectrum) will not experience the TIR when the waveguide incident angle approaches the critical angle. Also, with narrower incident angles, there is a greater portion of the transmission (cross) coupling component, which has inherently more loss compared to the reflection component, in the 3D versus 2D simulations. In order to maintain transmission (cross) coupling, the EBS gap must also be made narrower, which makes the fabrication more difficult. The narrower gaps suffer increasingly from fabrication imperfections, such as rough and sloped etch sidewalls and insufficient etch depth. Hence, there is a tradeoff between the simulated low insertion loss with larger incident angles and narrow gaps versus the insertion loss added from non-ideal fabrication. Here, we limited the inherent insertion loss to a maximum of ~2 dB by utilizing incident angles of 24° and 26°, 6° and 8° away from the critical angle respectively. The gap width was varied between 0.35 and 1.0 µm, with the narrowest gap limited by the fabrication process. The overall foot-print of the designed EBS coupler is 8x11 µm.

3. EBS fabrication

The main difficulty of realizing the proposed beam splitter lies in the definition and etching of the narrow high aspect ratio EBS gap with good quality. This implies no slanted or rough sidewalls and a sufficient etch depth that reaches through the waveguide layer. In addition, the fabrication complexity of the EBS should ideally be kept to a minimum to allow for easy integration with standard photonic integrated circuit (PIC) fabrication. For our deeply etched EBS coupler design, the EBS is simply patterned and etched together with all the other waveguide structures. This eliminates any alignment errors and adds minimal process steps. A standard i-line photolithographic process was used to pattern waveguides and all EBS gaps 400 nm and wider. However, due to this resolution limitation in our photolithographic capabilities the 350 nm EBS gaps were in this work defined using electron beam lithography (EBL). For the hard mask we use a bi-layer of 50 nm Cr on top of 500nm SiO_2. The EBL and photolithographic patterns are first etched separately into the Cr layer. The complete mask pattern is then transferred into the SiO_2, which acts as the hard mask for etching the semiconductor. In order to achieve anisotropic waveguides and EBS gaps, it is crucial that the SiO_2 hard mask has straight sidewalls, since any slope will subsequently transfer into the semiconductor due to mask degradation. We have developed a SF_6-Ar based inductively coupled plasma (ICP) etch that has good Cr to SiO_2 selectivity (30:1) and produces very straight SiO_2 sidewalls [17]. The ICP etching of InP/InGaAsP uses a Cl:H_2:Ar chemistry [17–19]. We have previously optimized conditions to yield very anisotropic and smooth deeply etched waveguides that demonstrate low propagation loss [20]. In order for the optical mode

#137249 - $15.00 USD Received 26 Oct 2010; revised 17 Dec 2010; accepted 22 Dec 2010; published 5 Jan 2011
(C) 2011 OSA

to experience FTIR in the EBS coupler, the etch must reach through the transverse waveguide layer inside of the EBS gap. However, like most reactive ion etching (RIE), there is an aspect ratio dependent etch rate (ARDE) that limits the etch depth inside of the narrow EBS gap. At the same time, for device integration, the upper waveguide cladding thickness is restricted by the layer structure in active regions. A ~1.6 µm cladding layer is necessary between the waveguide and the top InGaAs contact layer, to avoid absorption. Thus the etching of narrow and deep EBS gaps is especially difficult for active material integration platforms. In this work we solved this problem by implementing a novel pre-etching technique to counteract the ARDE effect of the EBS gaps. An area around the EBS coupler is etched prior to the waveguide and EBS patterning, decreasing the required etch depth of the EBS gaps, as shown in Fig. 3(a). The depth of this pre-etch is limited by two factors: first, the EBS and waveguides must be able to be patterned over the induced step height, and second, optical loss due to the change in optical mode profile at the interface must be avoided. Using a 950 nm thick photo-resist with contrast enhancer (SPR950CM with CEM365i) we found that the lithographic patterning is not compromised for step heights up to about 1 µm. Treating the waveguide discontinuity as a modal excitation problem, the interface loss is calculated to be small (–0.027 dB) for the 1.0 µm step. Still, in order to avoid detrimental back reflections, this interface is angled with respect to the propagation direction. The pre-etched region with successful patterning is demonstrated in Fig. 3(b). With this ~0.9 µm pre-etch, a reduced etch depth of 1.55 µm inside the EBS gap is required, in order to reach 300 nm below the waveguide layer.

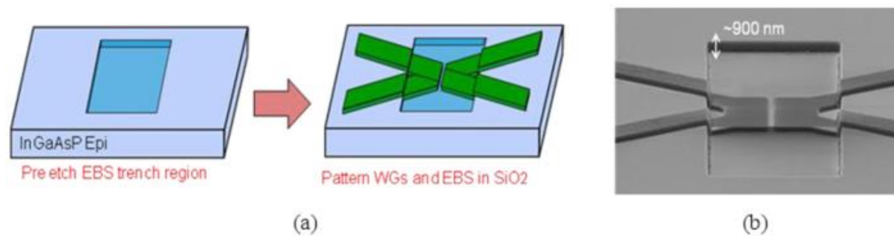

Fig. 3. (a) Schematic of pre-etching process. (b) Scanning electron microscopy (SEM) image of the hardmask illustrating the successful patterning over the pre-etched region.

The fabricated EBS coupler is shown in Fig. 4, the EBS gaps demonstrate smooth anisotropic sidewalls with a satisfactory etch depth even for the narrowest gaps. However, all EBS gaps are widened by about 70 nm in the ICP process. This is attributed to minor mask degradation together with a slow lateral etch rate.

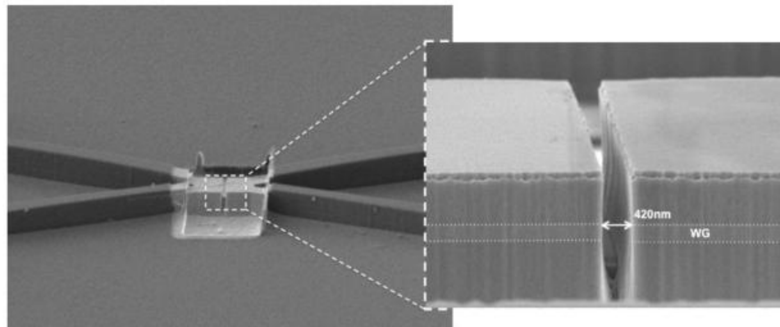

Fig. 4. SEM image of the EBS coupler. The lighter region shows where the SiN_x insulation layer was selectively removed to achieve a semiconductor-air interface in the EBS gap. The highlighted EBS gap demonstrates anisotropic and smooth sidewalls and a sufficient etch through the waveguide layer.

#137249 - $15.00 USD Received 26 Oct 2010; revised 17 Dec 2010; accepted 22 Dec 2010; published 5 Jan 2011
(C) 2011 OSA

For integration of the EBS coupler with standard InP/InGaAsP PICs, there is only a single added process step, besides the pre-thinning process described above. The nitride layer used for isolating metal contacts from the substrate needs to be selectively removed inside of the EBS gap in order to achieve FTIR. This was done by using a 7 µm thick resist (SPR220-7) to cover deep waveguides and metal contacts. Then selectively opening a region around the EBS coupler and using a high pressure (300 torr) CF_4 plasma etch to isotropically remove SiN_x around and inside the EBS gap, see Fig. 4.

In this work we incorporated: active gain, phase modulation and low loss passive waveguides, by utilizing an active/passive InP/InGaAsP offset quantum wells (OQW) integration platform [21]. Passive waveguide sections and phase modulator regions are here defined by selectively etching away the quantum wells. This is followed by a single blanket re-growth to provide p-cladding everywhere.

3. EBS characterization

The EBS coupler was characterized using a symmetric 4-port test structure shown in Fig. 5. Each of the waveguide arms around the EBS incorporates a semiconductor optical amplifier (SOA), used as an on-chip detector. The absolute power transmission and reflection components and the overall insertion loss of the EBS coupler can be accurately determined by fiber coupling an external tunable laser source and measuring the photocurrents on-chip. The input SOA is first used to measure the input light intensity. This input SOA is then biased at transparency and the light transmitted and reflected in the EBS coupler is measured by the SOAs in each waveguide arm. Since all the SOAs are identical, the measurement becomes insensitive to the responsivity of the SOAs. However, a separate test structure was however used to determine the wavelength dependent transparency current of the SOAs. Because of the small transmission components for some of the EBS designs, a lock-in approach was utilized to enhance signal-to-noise ratio (SNR) and separate the signal from the DC diode leakage current in the SOAs (~10µA). All measurements were done at room temperature and with TE-polarized light in order to interact with the compressively strained InGaAsP quantum wells [21]. Finally, to account for the passive waveguide sections around the EBS coupler, a 0.22 dB insertion loss was subtracted from the measured coupling powers. This number was determined from previous measurements of 2.1 cm^{-1} propagation loss in our deeply etched waveguides [20].

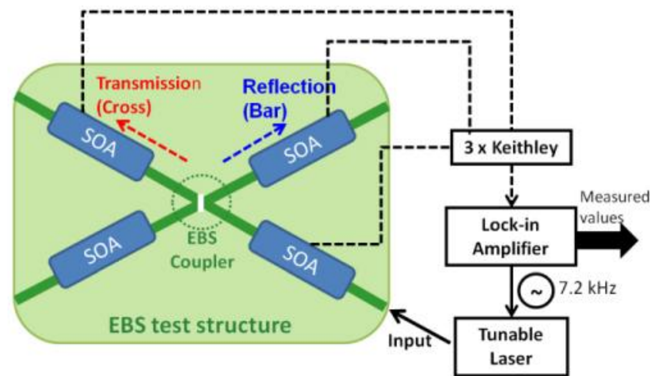

Fig. 5. Schematic of the test structure used for characterizing power coupling and insertion loss of the different EBS coupler designs. Lock-in at 7.2 kHz issued to improve sensitivity. On-chip SOAs are reversed biased to detect coupled light.

#137249 - $15.00 USD   Received 26 Oct 2010; revised 17 Dec 2010; accepted 22 Dec 2010; published 5 Jan 2011
(C) 2011 OSA

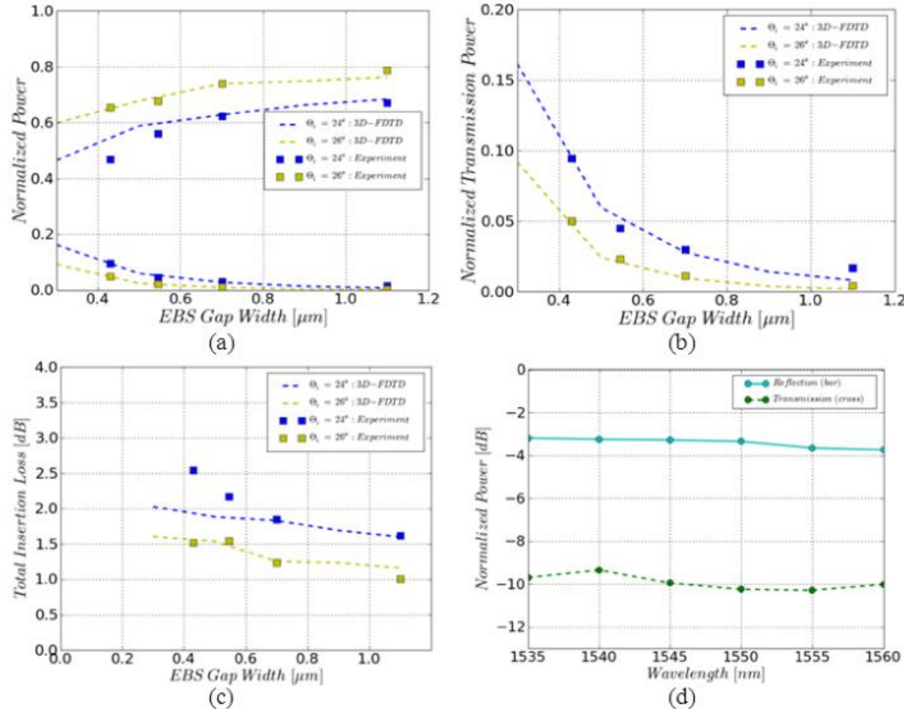

Fig. 6. (a),(b) EBS power coupling and (c) insertion loss as a function of gap width for incident angles (Θ_i) of 24° and 26° at 1550 nm, for measured EBS coupler designs (squares) and 3D-FDTD simulations (dashed lines). (d) Measured power coupling as a function of wavelength for the 80/20 (bar/cross) EBS design.

The experimentally measured coupling values and insertion loss of the EBS matches very well with the 3D-FDTD simulations, as demonstrated in Fig. 6(a,b,c). The largest transmission (cross) coupling design was the Θ_i = 24° with 0.42 µm air gap, which demonstrates an relative bar/cross coupling ratio of 80/20 and an overall insertion loss of 2.6 dB. The lowest insertion loss coupler design was the Θ_i = 26° with 1.1 µm air gap. This design demonstrates only 1.0 dB insertion loss, but has at the same time a very unequal bar/cross coupling ratio of 99.5/0.5. For WDM or other applications where a wide range of bandwidth is utilized, it is important that the coupling ratio and insertion loss does not change significantly with wavelength. We confirmed that the EBS coupler has a relatively weak wavelength dependence, as shown in Fig. 6(d). The reflection (bar) and transmission (cross) component for this 80/20 coupler varies only by <0.6 dB and <1.0 dB respectively over a 25 nm wavelength span in the C-band.

4. EBS couplers integrated with PICs

In order to further demonstrate the integration of the EBS coupler with the InP/InGaAsP integration platform, we designed and fabricated novel flattened ring resonator devices [13]. Figure 7 highlights the flattened ring design and how it offers a larger bending radius for a fixed resonator delay compared to a conventional circular design. An increased bending radius translates into a lower roundtrip loss, through reduced scattering and radiation loss. This becomes especially advantageous for micro-ring resonators where the bending radius needs to be very small. The resonator length (L) is defined by the incident angle (Θ_i) (in degrees) at the EBS coupler together with the bend radius (R) of the waveguides: $L = \Theta_i R\pi / 45$. The fabricated device in Fig. 7 utilizes the flattened ring resonator with a Θ_i = 24° / 0.5 µm EBS coupler design and a bending radius of 500 µm, giving a resonator

#137249 - $15.00 USD Received 26 Oct 2010; revised 17 Dec 2010; accepted 22 Dec 2010; published 5 Jan 2011
(C) 2011 OSA

circumference of 838 μm. The resonator incorporates a 375 μm SOA and two phase modulators (PM). In addition to the flattened resonator, the device also includes a Mach-Zehnder interferometer (MZI). Such a device could be used as the basic building block for higher order lattice filters [22].

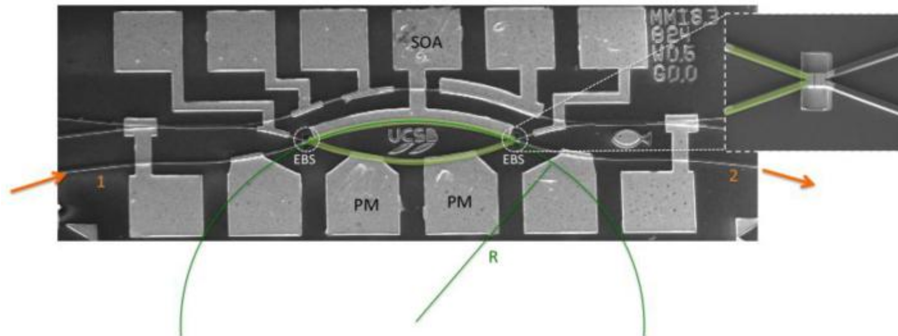

Fig. 7. SEM image of a PIC filter device that utilize the flattened ring resonator design with EBS couplers. Highlighted waveguides shows the flattened ring and illustrates the reduction in resonator length versus a circular resonator design. Port 1 and 2 shows the input and output waveguide ports for the measured filter responses.

Here we use the single resonator to demonstrate a tunable channelizing filter device. The filter function is measured by sweeping the wavelength of an external tunable laser and locking in the signal using an on-chip reversed biased phase modulator after the resonator. Figure 8 shows the measured filter responses. Adjusting the current to the SOA the pole-magnitude (*G*) of the filter response is tuned, this is demonstrated in Fig. 8(a) for *G*=0.5 and 0.75 for SOA biases of 15 and 20 mA respectively. The filter function fits well with the theoretical S_{21} parameter of an ideal resonator shown in the inset of Fig. 8(a). By utilizing the phase modulators, the filter can easily be shifted in wavelength, as verified in Fig. 8(b). Hence, using the SOA and PMs together the resonator poles can be placed anywhere in the complex plane. This demonstrates the basis of a very versatile channelizing filter. For better stopband rejections and flat-topped passbands, several stages should be cascaded to produce higher order filters [22]. For this application, the small cross-coupling provided by the EBS is ideal, as it allows for high finesse filters with large stopband rejections [23]

The flattened ring resonator can naturally also works as a laser if the SOA is biased at higher currents. The CW threshold for this device is 23 mA with single mode lasing and a side mode suppression ratio (SMSR) of ~32 dB demonstrated in Fig. 9.

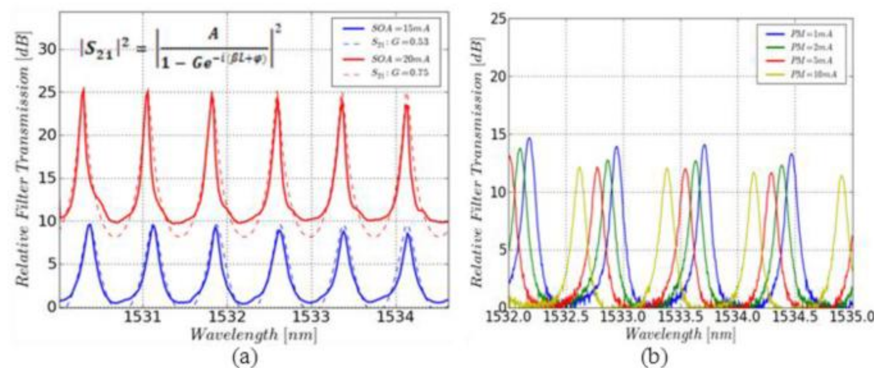

Fig. 8. Measured filter responses of the flattened ring resonator. (a) Tuning of pole-magnitude (G) by changing bias on the SOA (solid), with ideal simulated S_{21} filter function superimposed dashed). (b) Tuning of the filter center frequency by current injection in the phase modulators (PM).

#137249 - $15.00 USD Received 26 Oct 2010; revised 17 Dec 2010; accepted 22 Dec 2010; published 5 Jan 2011
(C) 2011 OSA

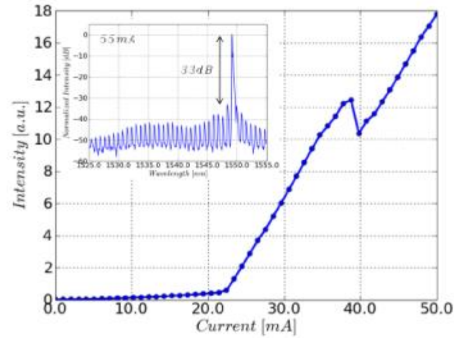

Fig. 9. Light-current characteristic of the flattned ring resonator demonstrating onset of lasing at ~23 mA, inset shows the lasing spectrum at 55mA, single mode operation with ~32 dB of SMSR.

5. Conclusion

We have reported on the design, integration and characterization of etched beam splitter (EBS) couplers in the InP/InGaAsP material system. For the design, 2D- and 3D-FDTD simulations were investigated and compared. It was concluded that the 2D case is useful for predicting trends although inaccurately predicting low insertion loss due to the ignoring of the transverse modal effects. EBS couplers with relatively low transmission components (≤ 10%) were preferred in order to limit inherent insertion loss (incident angles ≥ 24°) and provide realistic fabrication (EBS gaps ≥ 0.35 μm). Using a novel pre-thinning process and optimized ICP etching conditions for the InP/InGaAsP material system, EBS couplers were successfully realized. We note that the EBS does not add significant fabrication complexity to standard InP/InGaAsP PIC fabrication, granted EBL can be avoided. The EBS couplers were characterized using a robust test structure utilizing on-chip detectors, thus, eliminating any uncertainty in fiber-coupling. Measured power coupling ratios showed very close agreement with 3D-FDTD simulations. EBS couplers with transmission (cross) and reflection (bar) components of 0.5-10% and 44-80% respectively, were demonstrated. The foot-print of the coupler is 8x11 μm. Such couplers are useful for applications requiring compact foot-print and relatively large bar/cross coupling ratios including, low threshold ring lasers, and coupled ring filters, where in order to achieve a narrow passband the inter-ring coupling must be small. In this work we utilized the EBS coupler in a novel flattened ring resonator geometry. This resonator design offers an increased bending radius for a given resonator circumference, compared to conventional circular resonators; this translates into a lower bending loss. Utilizing the active gain and phase modulation offered by the InP/InGaAsP material system, a tunable channelizing filter as well as a ring laser was demonstrated.

Acknowledgements

This work was supported by DARPA under the PhASER program, a portion of this work was done in the UCSB nanofabrication facility, part of the NSF funded NNIN network.

#137249 - $15.00 USD Received 26 Oct 2010; revised 17 Dec 2010; accepted 22 Dec 2010; published 5 Jan 2011
(C) 2011 OSA